Available online at www.sciencedirect.com

ScienceDirect

Ceramics International 40 (2014) 1495–1502

CERAMICS INTERNATIONAL

www.elsevier.com/locate/ceramint

Effects of porosity and pore size on the properties of AgO-decorated porous diatomite ceramic composites

Wenning Shen*, Lajun Feng, Ali Lei, Zheng Liu, Yuanqing Chen

School of Materials Science and Engineering, Xi'an University of Technology, No. 5 South Jinhua Road, Xi'an 710048, China

Received 29 May 2013; received in revised form 5 July 2013; accepted 5 July 2013
Available online 16 July 2013

Abstract

Porous diatomite ceramics with different porosity and pore size were prepared by sintering compacts consisting of diatomite, different amounts of sodium carbonate or pore former with different particle size. Subsequently, AgO-decorated porous diatomite ceramic composites were synthesized by chemical oxidation using porous diatomite ceramics with different porosity and pore size as the carrier. The AgO contents of the composites were investigated as a function of porosity and pore size. The porosity and pore size of porous ceramics varied with the addition amount of sodium carbonate and particle size of pore former. The AgO content of the composites increased with the increase of the porosity. The pore size seriously influenced the content of AgO deposit on porous ceramics. When the pore size of porous ceramics was in the submicron range (< 1 μm), only a thin layer of submicron AgO particles could be deposited onto the external surface, but AgO particles could not further deposit into the inner layer. For pore formers smaller than 400 μm, the AgO contents of the composites increased with increasing size of pore former. However, the AgO content of the composites decreased when the size was larger than 400 μm. XRD results showed the composites were composed of cristobalite, tridymite, AgO and Ag_2O.

Keywords: B. Porosity; Diatomite; Porous ceramics; AgO; Pore size

1. Introduction

It is well known that silver or silver ions have a strong inhibitory effect to microbes and good bactericidal effects [1–3]. They can inhibit the growth of various microorganisms [4–9]. It is found that bacteria exhibit a low propensity to develop a resistance to silver-based products. Thus, silver-based materials can help to solve the problem of the growing microbial resistance against metal ions, and commonly used antibiotics [10–14]. The bactericidal effect of different Ag-containing materials is directly proportional to their valence. For example, the bactericidal effect of AgO with Ag^{2+} is superior to that of Ag_2O with Ag^{1+}, and elementary Ag shows an inferior bactericidal effect compared to AgO and Ag_2O [15–17]. Therefore, among different silver-based materials, AgO attracts great interests due to their great potential for antimicrobial applications [18–20].

In the past decades, nanoscale or submicron materials find wide application due to their size effects. Similarly, due to their high specific surface area and high fraction of surface atoms, submicron and nanoscale AgO particles show higher antimicrobial activity compared with bulk AgO particles [21,22]. However, when employed alone in water treatment, submicron and nanoscale particles are easily aggregated or lost in solution, leading to the deterioration of their chemical properties and the degradation of their antimicrobial activity [23–25]. To solve these problems, submicron and nanoscale AgO particles have been grafted onto porous diatomite ceramics [26]. In such a case, the degradation of chemical activity of the AgO particles caused by their aggregation can be effectively prevented, their loss can be greatly reduced, and hence excellent bactericidal effect can be achieved.

In general, for AgO-deposited porous ceramic composites, the higher the content of the AgO particles in the composite, the better the bactericidal effect. It has been found that the porosity, pore shape and pore size have a great influence on the properties of porous ceramics [27,28]. Thus, it can be expected that the content of the AgO may be closely related to the porosity and pore size of the porous ceramics. However, it has been seldom reported so far.

*Corresponding author. Tel.: +86 29 8231 2733, +86 13152075522; fax: +86 29 8231 2733.
E-mail addresses: shenwenning@qq.com (W. Shen), fenglajun@xaut.edu.cn (L. Feng).

0272-8842/$ - see front matter © 2013 Elsevier Ltd and Techna Group S.r.l. All rights reserved.
http://dx.doi.org/10.1016/j.ceramint.2013.07.034

In this study, porous diatomite ceramics with different porosity and pore size were fabricated by adding different amounts of sodium carbonate and different particle size of pore former. The dependence of the deposited AgO content on the porosity and pore size of the ceramic were investigated.

2. Material and methods

2.1. Materials

To prepare diatomite ceramics, diatomite powders (chemical purity, Tianjin Tianda Chemical Reagent Plant) with a mean particle size of 26.7 μm and a size distribution of 0.7–180 μm (diatomite was distributed in deionized water and measured by a BT-2003 laser particle sizer) were used as source material. Anhydrous sodium carbonate (analytic purity, Tianjin Northern Tianyi Chemical Reagent Plant), polyacrylamide and polyvinyl alcohol (analytical purity, Tianjin Kermel Chemical Reagent Co., Ltd.), and commercial available polystyrene foam (chemical purity) were used as fusing agent, dispersant, binder and pore former, respectively. Silver nitrate (analytical purity, Xi'an Non-ferrous Metals Research Institute), potassium persulfate and potassium hydroxide (analytical purity, Tianjin Tianli Chemical Reagent Co., Ltd.) were used as reactants during the synthesis of AgO decorated porous ceramic composites. Manganese sulfate (analytical purity, Tianjin Taixing Reagent Factory), phosphoric acid (analytical purity, Chengdu Kelong Chemical Reagent Factory), ammonium ferrous sulfate (analytical purity, Tianjin Tianhe Chemical Reagent Factory), and N-phenylanthanilic acid (analytical purity, Chengdu Jinshan Chemical Reagent Factory) were employed to determine the AgO content of the composites. Deionized water was self-made in our laboratory.

2.2. Preparation of porous diatomite ceramics

Porous diatomite ceramics were prepared by solid-state sintering. Diatomite powders were washed with deionized water, and then filtrated to remove fines and other adhered impurities. After that, the diatomite powders were calcined in a muffle furnace at 550 °C for 2 h. Subsequently, the diatomite powders were mixed with different additives to prepare porous ceramics with different porosity and pore size. To prepare the ceramic matrix with different porosity, Na_2CO_3 was used as fusing agent and mixed with the pretreated diatomite powders and polyacrylamide (PAM, 0.6 wt%). Five kinds of mixtures (MA1, MA2, MA3, MA4, and MA5) with different weight percentage of Na_2CO_3 (7 wt%, 10 wt%, 13 wt%, 16 wt% and 19 wt%, respectively) were obtained. To prepare the ceramic matrix with different pore size, polystyrene as a pore former was added into the mixture of diatomite powders, polyacryl amide (PAM, 0.6 wt%), and Na_2CO_3 (13 wt%). Using polystyrene (PS) with diameter of 83, 200, 300, 400 and 500 μm as a pore former, five kinds of mixtures (MB1, MB2, MB3, MB4 and MB5) with different pore size were obtained.

The mixtures (MA1-5 and MB1-5) were then ball milled for 6 h with zirconia balls as the grinding media. After that, they were mixed with 0.6 wt% polyvinyl alcohol (PVA) liquid (weight ratio of 40/60), resulting in a well-dispersed slurry. The slurry was squeezed out to form a cylindrical sample with diatomite of 6 mm under a pressure of 0.5 MPa. For comparison, the mixture MA2 was also pressed under a high pressure of 6.4 MPa. The samples were then dried at 50 °C for 6 h, and fired at 300 °C to burn out of the PS. Finally, the compacts were sintered in a alumina crucible at 1000 °C for 2 h, resulting in ceramic matrix samples of CA1, CA2, CA3, CA4, and CA5 (produced from MA1–5, correspondingly), CA21 (produced from MA2 under a pressure of 6.4 MPa), and CB1, CB2, CB3, CB4, and CB5 (produced from MB1-5, respectively).

2.3. Synthesis of AgO-decorated porous diatomite ceramic composites

AgO-decorated porous diatomite ceramic composites were prepared by direct chemical oxidation. Specifically, the obtained ceramic matrices were separately immersed in 25 mL of 1.5 mol/L $AgNO_3$ solutions for 96 h at room temperature. After filtration, Ag-decorated porous ceramic composites were obtained. The amount of Ag^+ in the porous ceramics was measured according to the Volhard method [29]. The obtained Ag-decorated ceramic was then utilized to prepare AgO-deposited porous ceramic composites through the following process. Firstly, 100 mL of $K_2S_2O_8$ solutions and 50 mL of KOH solutions were prepared in advance. The molar ratios of $K_2S_2O_8$ to adsorptive Ag^+ and that of KOH to adsorptive Ag^+ were controlled at 3:1 and 5.5:1, respectively. Secondly, the prepared aqueous solution of $K_2S_2O_8$ was transferred to a 500 mL glass round-bottomed flask, which was then heated up to 60 °C. The Ag-decorated ceramics were then added into the aqueous solution of $K_2S_2O_8$. During this process, the KOH solution was added into the reaction solution quickly after the ceramic particle surface were observed to become black. Thirdly, the flask was placed in a constant temperature oscillator at 60 °C and oscillated for 1 h at a speed of 200 r/min; finally, the solid product was obtained by filtration. The AgO-decorated porous ceramic composites were ready after the solid product was washed with deionized water and then dried at 70 °C for 4 h.

2.4. Characterization

The density and porosity of the ceramic matrices and AgO-decorated porous ceramic composites were measured by using the water displacement method based on the Archimedean principle.

The mass contents of the AgO in the prepared composites were measured according to the Mn^{2+} oxidation-reduction method [30]. The formula is as follows:

$$\omega(\mathrm{AgO}) = \frac{0.028 \times V \times 123.83}{1000m} 100\% \quad (1)$$

where V is the consumed volume of the standard ammonium ferrous sulfate solution (mL), and m is the mass of AgO-decorated porous ceramic composites (g).

The ceramic matrices and prepared composites were analyzed by XRD-7000S X-ray diffractometer (XRD). XRD data were

collected at room temperature with an X-ray source for Cu Kα radiation ($\lambda = 0.15418$ nm). Additional acquisition parameters were: tube voltage, 40 kV; tube current, 40 mA; 2θ range, 10–80°; and scan speed, 10°/min. The relative mass fraction of cristobalite phase and tridymite phase in the ceramic matrix is calculated in terms of the relative intensity of maximum cristobalite phase peak (101) and maximum tridymite phase peak (100) [31], as indicated by the formula (2).

$$\omega_{\text{cristobalite}} = \frac{1}{1 + 1.817(I_{\text{tridymite}}/I_{\text{cristobalite}})} \times 100\%, \quad (2)$$

where $\omega_{\text{cristobalite}}$ is the content of cristobalite phase in the ceramic matrix, $I_{\text{cristobalite}}$ is the relative intensity of maximum cristobalite phase peak (101), and $I_{\text{tridymite}}$ is the relative intensity of maximum tridymite phase peak (100). The content of tridymite phase is $1 - \omega_{\text{cristobalite}}$.

The microstructures and morphologies of the ceramic matrices were observed using a JSM-6700F scanning electron microscope (SEM) equipped with an Oxford INCA X-ray energy dispersive spectrometer (EDS) at an accelerating voltage of 20 kV. For SEM analysis, a thin film of Pt was sputtered on the sample surface. The amplified morphologies of the samples were observed by a 7SZ-405 video stereomicroscope.

3. Results and discussion

3.1. Microstructure and morphology

Fig. 1 shows SEM images of the ceramic matrices. It can be seen that for all the ceramic matrices, macropores were formed in the ceramics after sintering, and the pore shape was irregular. The ceramic matrix CA21, fabricated under a pressure of 6.4 MPa, was denser than those prepared under a pressure of 0.5 MPa. The pore size of the ceramic matrix CA21 was around 1 μm, while those of the ceramic matrix CA3 and CB2 with sodium carbonate and pore former additions were in the range of 10–200 μm. The pore size of the ceramic matrices prepared under low pressure was much larger than that of the ceramic matrix prepared under higher pressure.

Fig. 2(a) shows SEM micrograph of the composite prepared by decorating AgO particles on the ceramic matrix CA21. The pore size of the composite was around 5 μm, which was smaller than that of its corresponding ceramic matrix. Moreover, there were submicron particles depositing on the ceramic matrix. EDS analysis was made on the surface marked with pane 1 in Fig. 2(a) and the result is shown in Fig. 2(b). There mainly were elements Ag, Si, O and C, and the atomic percentages of these elements were 28.6%, 10.4%, 55.8% and 5.2% respectively. The element C might result from the reaction between surface oxygen atoms and atmospheric CO_2. It was a common characteristic for all silver oxides. This result proved that element Ag had been deposited onto the ceramics. Besides, the O/Si atomic ratio (5.4) exceeded the theoretical value (2). This indicated that the particles deposited onto the pore surface might be silver oxide.

The vertical section amplified morphologies of the composites prepared by decorating AgO particles on the ceramic matrix CA21 and CA2 are shown in Fig. 3. For the ceramic matrix CA21, only a thin layer on the external surface of the ceramic matrix turned gray black after AgO deposition, while

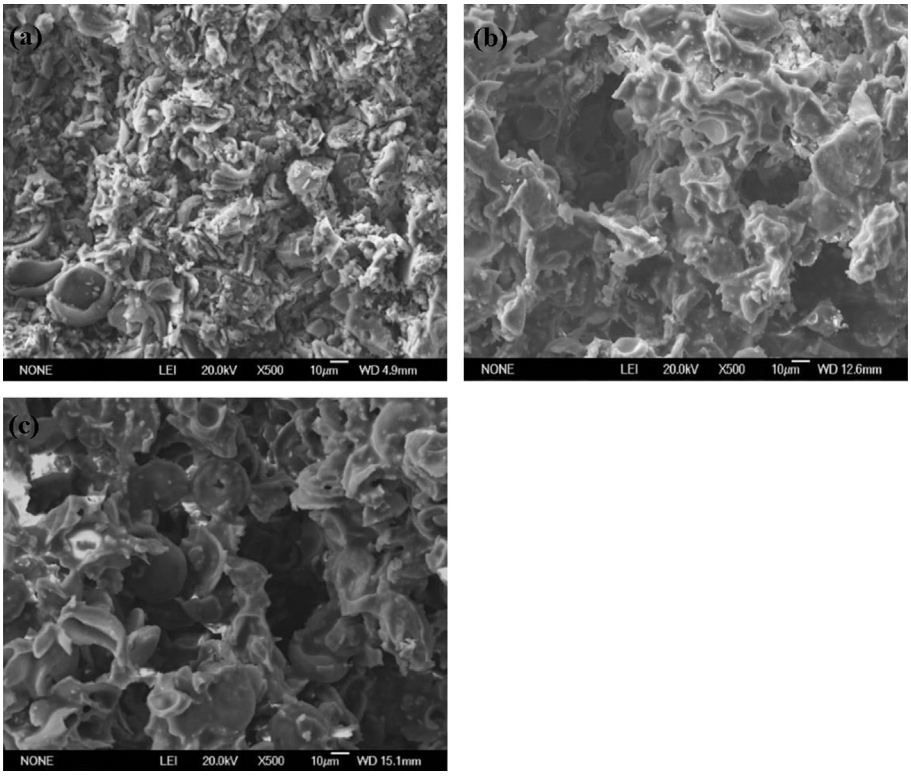

Fig. 1. SEM micrographs of the ceramic matrices, (a) CA21, porosity: 62.1%; (b) CA3, porosity: 64.2%; and (c) CB2, porosity: 61.6%.

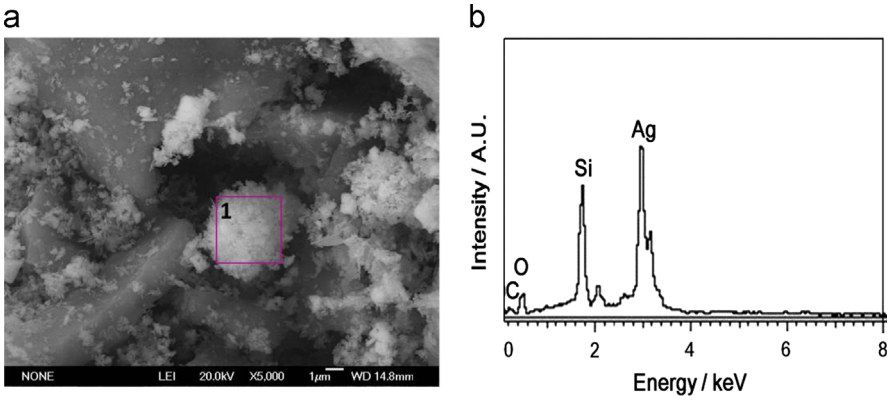

Fig. 2. SEM micrograph (a) and local EDS analysis result (b) of the composites obtained by decorating AgO particles on the ceramic matrix CA21.

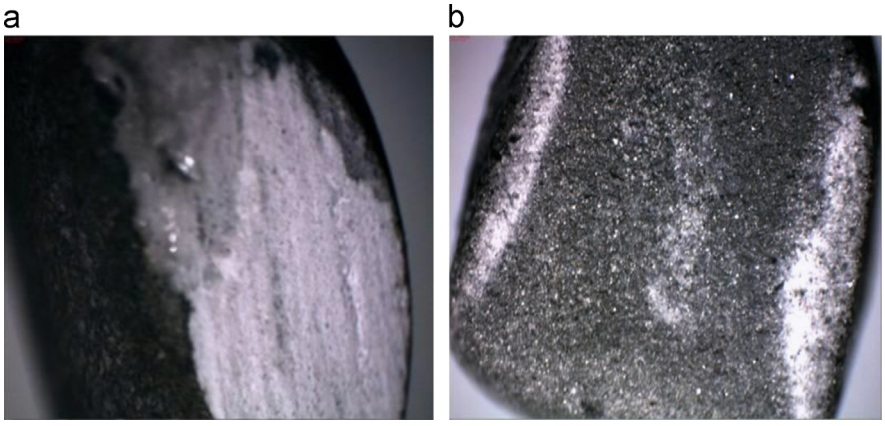

Fig. 3. Amplified morphologies of the composites prepared by decorating AgO particles (a) on the ceramic matrix CA21 and (b) the ceramic matrix CA2.

the inner layer was still white. But for the ceramic matrix CA2, most parts of the ceramics turned gray black. The color of the composites might derive from the deposition of submicron AgO particles or Ag_2O nanoparticles, since silver nanoparticles are of yellowish brown color [32], Ag_2O nanoparticles are of brownish black color [33], and AgO submicron particles are of black color [34]. This result indicated that the pore size would affect the AgO particles depositing on the ceramic matrix. It is because that the pore size of the ceramic matrix CA21 prepared under high pressure was smaller. The smaller the pore size is, the larger is the Ag^+ adsorption amount on the ceramic matrix. However, submicron AgO particles formed by oxidation filled up the pores on the external surface and prevented further oxidation of Ag^+ in the inner layer.

3.2. Porosity

The pores in the ceramic matrices are formed after the powder mixture is sintered. The porosity and pore size of the ceramic matrices are closely related to the content of carbonate and the diameter of pore former (polystyrene) in the mixture. Fig. 4 shows the dependence of porosity of the ceramic matrix on the content of sodium carbonate (Fig. 4a), and on the diameter of pore former (Fig. 4b). Obviously, the porosity of the matrix decreased with an increase in the content of sodium carbonate. This result showed that porosity was determined by the content of sodium carbonate. However, for the ceramic matrix prepared with the pore former of different size, almost no change of the porosity can be observed. This indicated that the size of pore former had little effect on the porosity. In addition, the porosity of the ceramic matrix CA21 prepared under a high pressure of 6.4 MPa was 62.1%, which was close to that of the ceramic matrix CA3 prepared under a pressure of 0.5 MPa.

Using the matrix samples (CA1–CA5) and (CB1–CB5), AgO-decorated porous ceramic composites (sample AgOCA1–AgOCA5 and AgOCB1–AgOCB5) were then obtained. The porosity of the highly AgO-decorated porous ceramic composite was lower than its corresponding matrix sample, as shown in Table 1, due to the fact that AgO particles were coated on the inner side of pores, thus reducing the pore volume. However, the change of the ceramic porosity during the process of AgO decoration shows a close relationship to the diameter of the pore former, as shown in Table 2. For example, when the diameter of pore former was 83 μm, the porosity was decreased from 60.0% of the matrix to 58.0% of the AgO-decorated ceramic composite. However, when the pore former with diameter of 400 μm was used, the porosity was decreased from 59.6% of the matrix to 51.4% of the AgO-decorated ceramic composite. It might be caused by the pore size of the

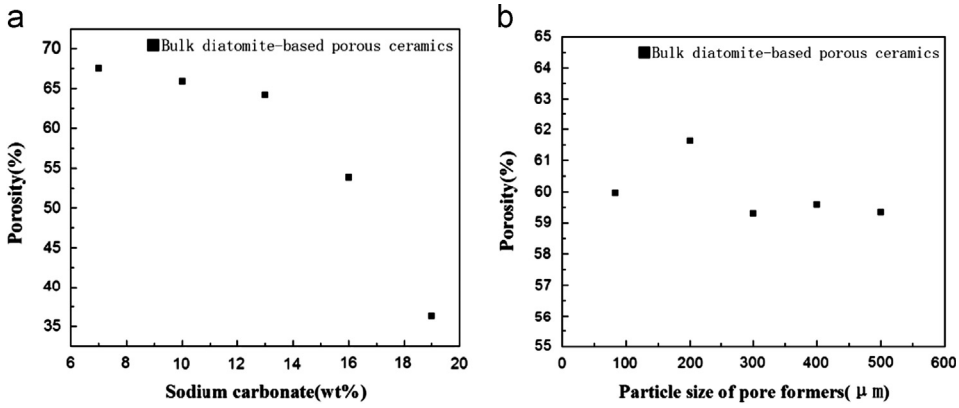

Fig. 4. Porosity of the ceramic matrices as a function of (a) the content of sodium carbonate and (b) the size of pore former.

Table 1
Porosity of the composites as a function of the porosity of their corresponding matrices.

Blank ceramic matrix	CA1	CA2	CA3	CA4	CA5
Porosity (%)	67.6	65.9	64.2	53.9	36.3
AgO-decorated ceramic composites	AgOCA1	AgOCA2	AgOCA3	AgOCA4	AgOCA5
Porosity (%)	57.3	54.4	43.7	30.4	25.3

matrix. For the diameter of pore former lower than 300 μm, the pore of the ceramic matrix was smaller. The AgO particles filled up and closed the smaller pores of the outer layer, inhibiting further AgO deposition on the pores of inner side. However, when the diameter of pore former was over 300 μm, the pores of the ceramic matrix became larger, and more AgO particles could deposit on the inner side of pores, resulting in the great reduction of the pore volume.

3.3. The AgO content of the composites

Fig. 5 shows the AgO content of the composites as a function of porosity. The AgO content increased with porosity. The rate of the AgO content increase in the composites was slow with the porosity of their corresponding ceramic matrices below 60%. However, above 60%, a rapid increase of AgO content in the composites was observed. For the same pore size of ceramic matrix, the adsorbability of Ag^+ is determined by the porosity of the ceramic matrix. The highly porous structures greatly increased the contacting area of the ceramic matrix with $AgNO_3$ solution, making more Ag^+ adsorbed on the ceramic matrix. The molecular surface of the ceramic matrix was subjected to more unbalanced forces with the increasing porosity, causing more Ag^+ adsorbed onto the ceramic matrix. Thus, the larger the porosity, the more the Ag^+ would be adsorbed, which had been confirmed by the tested adsorption amount of Ag^+ on the ceramic matrix after soaking for 96 h (Table 3). Moreover, the higher the porosity, the easier it is for the persulfate ions to enter the pores in the inner layers to oxidize Ag^+ and form submicron AgO particles. In other words, the combined action of Ag^+ adsorption degree and the difficult degree of oxidant entering the ceramic matrix resulted in the increase of AgO content in the composites with increasing porosity.

In order to confirm the effect of pore size on the AgO deposition, submicron AgO particles were separately decorated on the ceramic matrix CA21 and CA3. The AgO content of the composites was studied. The results showed that the adsorption amount of Ag^+ on the ceramic matrix CA21 and CA3 were 1.79 mmol/g and 1.59 mmol/g respectively, while the AgO content of the corresponding composites were 1.39% and 5.55% after oxidation. Since the pores of the ceramic matrix CA21 were relatively smaller and the ceramics were denser, the Ag^+ adsorbing capability of the ceramic matrix CA21 was stronger than that of the ceramic matrix CA3. However, the submicron AgO particles formed from oxidation blocked the smaller pores, hindering further entering of persulfate ions into the pores to oxidize Ag^+. But for the ceramic matrix prepared under lower pressure, as the pore was larger, it could not be filled up by the newly generated submicron AgO particles completely. Thus, persulfate ions could continue to enter the inner layers of the ceramic matrix to oxidize more Ag^+, resulting in the higher AgO content of the composites.

To further prove the effect of pore size, the AgO contents of the composites were studied by decorating AgO particles on the ceramic matrices CB1–5 prepared with different diameters of pore former, as shown in Fig. 6. It can be seen from Fig. 6 that the size of pore former significantly influenced the AgO content of the composites. For the diameter of pore former from 83 μm to 400 μm, the AgO content of the composites increased. However, above 400 μm, the AgO content of the composites decreased. The results suggest that the formation of AgO particles onto the ceramic matrix was likely to be affected by the pore size of the ceramic matrix. When the diameter of pore former was over 400 μm, the pore size of the sintered ceramic matrix was larger. The larger pore was beneficial to the entering of persulfate ions, but reduced the adsorption amount of Ag^+, leading to the decrease of AgO content of the composites.

3.4. XRD analysis

Fig. 7 shows XRD patterns of the ceramic matrices sintered at 1000 °C. It is noted that both cristobalite and tridymite occurred in all sintered ceramic matrices. No other phase was detected. The phase fraction of the ceramic matrix was calculated according to Eq. (2) [31], as shown in Table 4. The content of sodium carbonate

Table 2
Porosity of the composites as a function of the pore size of their corresponding matrices.

Size of pore former (μm)	80	200	300	400	500
Porosity of blank ceramic matrix (%)	60.0	61.6	59.3	59.6	59.3
Porosity of the composites (%)	58.0	59.4	55.1	51.4	52.8

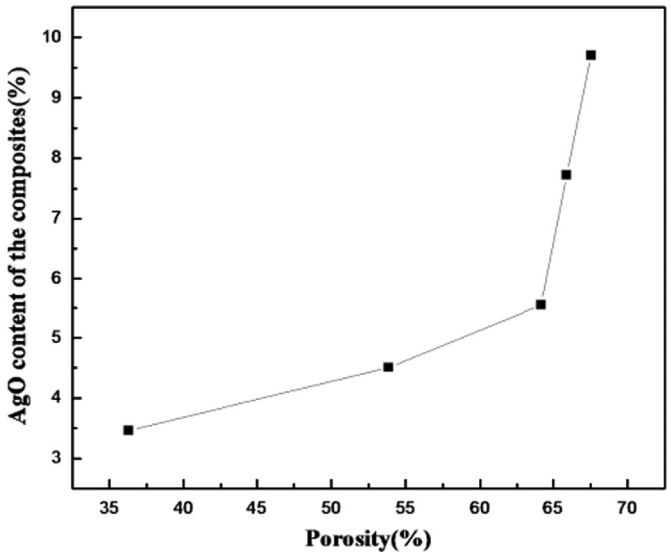

Fig. 5. Effect of the porosity on the AgO content of AgO-decorated ceramic composites.

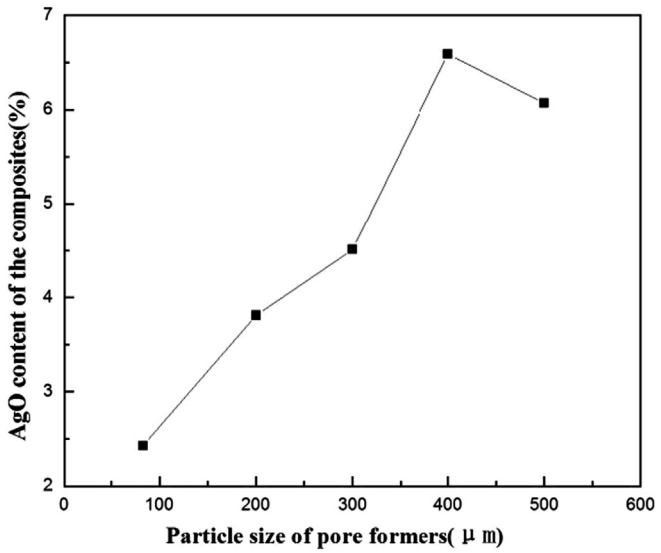

Fig. 6. Effects of the diameter of pore former on the AgO content of the AgO-decorated ceramic composites.

Table 3
Ag^+ adsorbed amount on the ceramic matrix with different porosity after soaking in $AgNO_3$ solution for 96 h.

Blank ceramic matrix	CA1	CA2	CA3	CA4	CA5
Porosity (%)	67.6	65.9	64.2	53.9	36.3
Ag^+ adsorbed amount (mmol/g)	2.15	1.79	1.59	1.35	1.24

and the diameter of pore former had an influence on the phase fraction of cristobalite and tridymite. The cristobalite phase content decreased with increasing content of sodium carbonate. Since the decomposition reaction of sodium carbonate is an endothermic reaction, the heat needed for the decomposition increased with the content of sodium carbonate. Thus, the interior temperature of sintered ceramic matrix was lowered, resulting in the reduction of phase transition rate. In addition, the cristobalite phase content increased with increasing diameter of pore former. It might be because that the pore size of sintered ceramic matrix increased with the pore former size, which was beneficial to the heat transfer. Thus, an interior temperature rise of sintered ceramic matrix occurred, promoting the transformation of tridymite to cristobalite.

Fig. 8 shows XRD patterns of the composites prepared by decorating AgO particles on different ceramic matrices. After being deposited with submicron AgO particles, cristobalite and tridymite occurred in all prepared composites as well as another phase. The diffraction peaks at 32.151°, 32.395°, 34.195°, 37.216°, 39.498° and 53.980° could be indexed to

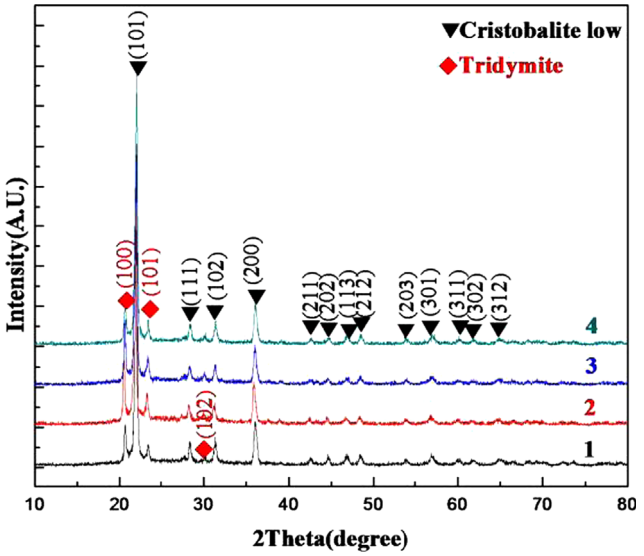

Fig. 7. XRD patterns of the ceramic matrices with different porosity and pore size. 1—CA2; 2—CA4; 3—CB2; 4—CB4.

the (200), (−111), (002), (111), (−202) and (−311) planes of monoclinic AgO. The diffraction peak at 32.630° in the XRD pattern might refer to the crystal face of cubic Ag_2O (111), but the other three strong diffraction peaks of Ag_2O did not appear. The results indicate that the element Ag of the composites existed in the form of AgO and a little Ag_2O after oxidation. Therefore, it can be concluded that it was possible

Table 4
Phase fraction of the ceramic matrices prepared under different conditions.

Samples	The ceramic matrix CA2	The ceramic matrix CA4	The ceramic matrix CB2	The ceramic matrix CB4
Content of cristobalite (%)	84.2	68.5	67.3	79.3
Content of tridymite (%)	15.8	31.5	32.7	20.7

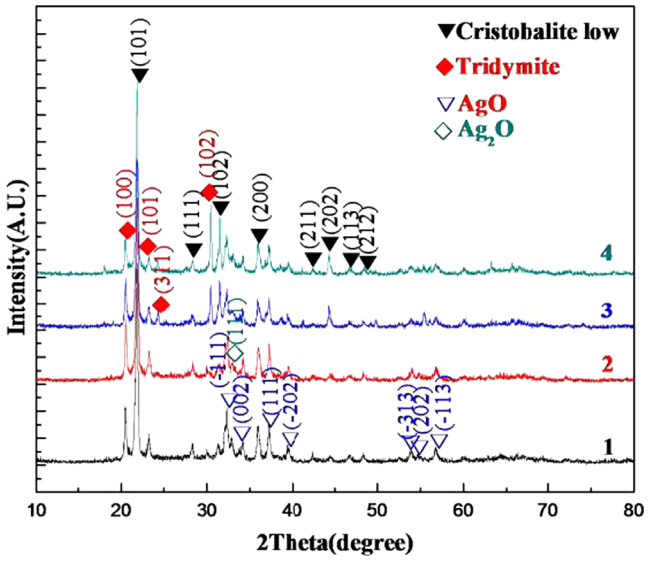

Fig. 8. XRD patterns of the composites prepared by decorating AgO particles on the ceramic matrix CA2, CA4, CB2 and CB4. 1-Sample AgOCA2, porosity of CA2: 65.9%; 2-Sample AgOCA4, porosity of CA4: 53.9%; 3-Sample AgOCB4; 4-Sample AgOCB2.

Table 5
Relative strength of the strongest peak of each phase in the composites.

Samples	AgOCA2	AgOCA4	AgOCB4	AgOCB2
$I_{\text{cristobalite (101)}}$	100	100	100	100
$I_{\text{tridymite (100)}}$	14	30.8	24.4	18.8
$I_{\text{AgO (−111)}}$	29.8	20.0	19.5	17.4
$I_{\text{Ag}_2\text{O (111)}}$	10.6	7.6	4.9	7.3

to directly generate AgO particles on the ceramic matrices through chemical oxidation. Table 5 shows the relative intensity of the strongest diffraction peaks for each phase of the composites in the XRD patterns. For the samples AgOCA2 and AgOCA4, with increasing porosity of the ceramic matrix, the relative intensity of the strongest AgO diffraction peak was stronger. For the samples AgOCB2 and AgOCB4, the larger the pore former size was, the stronger was the relative intensity. It is pointed out by diffraction intensity theory that the diffraction intensity of a phase is strengthened as the relative content of this phase increases in the composite [31]. Thus, it can be inferred that the AgO content of the ceramic matrix with higher porosity was larger than that of the ceramic matrix with lower porosity. For the composites prepared by decorating AgO particles on the ceramic matrix CB2 and CB4, the AgO content deposited on the ceramic matrix CB4 was higher than that deposited on the ceramic matrix CB2. This result further confirmed the determined AgO content.

4. Conclusions

Porous diatomite ceramics with different porosity and pore size have been prepared by adding different content of sodium carbonate and different particle size of pore former and sintered at 1000 °C over a range of porosity (36.0–68.0%). The effects of porosity and pore size on the properties of AgO-decorated porous ceramic composites were investigated. The porosity of the ceramic matrix increased with the content of sodium carbonate, and the increased porosity resulted in an increase in the AgO content of the prepared composites. Compared with their corresponding ceramic matrices, the porosity of the composites decreased after the decoration of submicron AgO particles. For the pore size less than micron range, only a thin layer of AgO particles could be deposited on the external surface of the ceramic matrices, while Ag^+ in the inner layers could not be oxidized. As the size of pore former increased, the AgO content of the composites increased. However, when the diameter of pore former was larger than 400 μm, the silver ion adsorption capacity of sintered ceramic matrices and the AgO content of the composites decreased.

Acknowledgments

This work was supported financially by the Science and Technology Planning Project of Xi'an, the Special Research Project of Education Department of Shaanxi Province of China and theExcellent Doctor Degree Dissertation Research Foundation of Xi'an University of Technology.

References

[1] V. Shashikala, V. Siva Kumar, A.H. Padmasri, B. David Raju, S. Venkata Mohau, P. Nageswara Sarma, K.S. Rama Rao, Advantages of nano-silver–carbon covered alumina catalyst prepared by electro-chemical method for drinking water purification, Journal of Molecular Catalysis A: Chemical 268 (2007) 95–100.
[2] H.J. Park, J.Y. Kim, J. Kin, J.H. Lee, J.S. Hahn, M.B. Gu, J. Yoon, Silver-ion-mediated reactive oxygen species generation affecting bacter-icidal activity, Water Research 43 (2009) 1027–1032.
[3] M. Rai, A. Yadav, A. Gade, Silver nanoparticles as a new generation of antimicrobials, Biotechnology Advances 27 (2008) 76–83.
[4] W.N. Shen, L.J. Feng, H. Feng, A.L. Lei, Divalent silver oxide-diatomite hybrids: synthesis, characterization and antibacterial activity, Ceramics International 39 (2013) 5013–5024.
[5] A.T. Le, P.T. Huy, P.D. Tam, T.Q. Huy, P.D. Cam, A.A. Kudrinskiy, Y. A. Kudrinskiy, Green synthesis of finely-dispersed highly bactericidal silver nanoparticles via modified Tollens technique, Current Applied Physics 10 (2010) 910–916.
[6] G. Gosheger, J. Hardes, H. Ahrens, A. Streitburger, H. Buerger, M. Erren, A. Gunsel, F.H. Kemper, W. Winkelmann, C.V. Eiff, Silver-coated mega-endoprostheses in a rabbit model-an analysis of the infection rate and toxicological side effects, Biomaterials 25 (2004) 5547–5556.

[7] C.M. Betbeze, C.C. Wu, S.G. Krohne, J. Stiles, In vitro fungistatic and fungicidal activities of silver sulfadiazine and natamycin on pathogenic fungi isolated from horses with keratomy cosis, American Journal of Veterinary Research 67 (2006) 1788–1793.
[8] J.L. Elechiguerra, J.L. Burt, J.R. Morones, A. Camacho-Bragado, X.X. Gao, H.H. Lara, Interaction of silver nanoparticles with HIV-1, Journal of Nanobiotechnology 3 (2005) 1–10.
[9] S.S. Mahapatra, N. Karak, Silver nanoparticle in hyperbranched polyamine: synthesis, characterization and antibacterial activity, Materials Chemistry and Physics 112 (2008) 1114–1119.
[10] F. Mirzajani, A. Ghassempour, A. Aliahmadi, M.A. Esmaeili, Antibacterial effect of silver nanoparticles on *Staphylococcus aureus*, Research in Microbiology 162 (2011) 542–549.
[11] J.R. Morones, J.L. Elechiguerra, A. Camacho, K. Holt, J.B. Kouri, J.T. Ramirez, M.J. Yacaman, The bactericidal effect of silver nanoparticles, Nanotechnology 16 (2005) 2346–2353.
[12] A. Panacek, M. Kolar, R. Vecerova, R. Prucek, J. Soukupova, V. Krystof, P. Hamal, R. Zboril, L. Kvitek, Antifungal activity of silver nanoparticles against *Candida spp*, Biomaterials 30 (2009) 6333–6340.
[13] K. Chamakura, R. Perez-Ballestero, Z.P. Luo, S. Bashir, J.B. Liu, Comparison of bactericidal activities of silver nanoparticles with common chemical disinfectants, Colloids and Surfaces B Biointerfaces 84 (2011) 88–96.
[14] B. Thati, A. Noble, R. Rowan, B.S. Creaven, M. Walsh, M. McCann, Mechanism of action of coumarin and silver(I)-coumarin complexes against the pathogenic yeast *Candida albicans*, Toxicology in Vitro 21 (2007) 801–808.
[15] H. Yang, K. Wang, X.G. Ding, G.Y. Zhou, M.Z. Ge, Study on relationship between antibacterial property and silver ions in inorganic antibacterial powders, Journal of Chinese Ceramic Society 30 (2002) 585–588 (in Chinese).
[16] P. Lalueza, M. Monzon, M. Arruebo, J. Santamaria, Bactericidal effiects of different silver-containing materials, Materials Research Bulletin 46 (2011) 2070–2076.
[17] W.N. Shen, L.J. Feng, Z.Z. Kong, H. Feng, Ultrafine silver peroxide powders prepared by ozone oxidization method and its antibacterial property, Acta Chimica Sinica 69 (2011) 277–283 (in Chinese).
[18] A.R. Shahverdi, A. Fakhimi, H.R. Shahverdi, S. Minaian, Synthesis and effect of silver nanoparticles on the antibacterial activity of different antibiotics against *Staphylococcus aureus* and *Escherichia*, Nanomedicine: Nanotechnology, Biology and Medicine 3 (2007) 168–171.
[19] F. Martinez-Gutierrez, P.L. Olive, A. Banuelos, E. Orrantia, N. Nino, E.M. Sanchez, F. Ruiz, H. Bach, Y. Av-Gay, Synthesis, characterization, and evaluation of antimicrobial and cytotoxic effect of silver and titanium nanoparticles, Nanomedicine: Nanotechnology, Biology and Medicine 6 (2010) 681–688.
[20] Q. Li, K. Chen, L.L. Jiao, G.G. Zhou, The preparation of the dispersed liquid of nanometer bivalent silver oxide, Water Purification Technology 27 (2008) 12–15 (in Chinese).
[21] Y.H. Kim, D.K. Lee, H.G. Cha, C.W. Kim, Y.S. Kang, Synthesis and characterization of antibacterial Ag–SiO_2 nanocomposite, Journal of Physical Chemistry C 111 (2007) 3629–3635.
[22] S.K. Rastogi, V.J. Rutledge, C. Gibson, D.A. Newcombe, J.R. Branen, A. Larry Branen, Ag colloids and Ag clusters over EDAPTMS-coated silica nanoparticles: synthesis, characterization, and antibacterial activity against *Escherichia coli*, Nanomedicine: Nanotechnology, Biology and Medicine 7 (2011) 305–314.
[23] C.L. Wang, J.T. Yan, X.J. Cui, H.Y. Wang, Synthesis of raspberry-like monodisperse magnetic hollow hybrid nanospheres by coating polystyrene template with Fe_3O_4@SiO_2 particles, Journal of Colloid and Interface Science 354 (2011) 94–99.
[24] W.N. Shen, L.J. Feng, H. Feng, Z.Z. Kong, M.J. Guo, Ultrafine silver(II) oxide particles decorated porous ceramic composites for water treatment, Chemical Engineering Journal 175 (2011) 592–599.
[25] O. San, R. Goren, C. Ozgur, Purification of diatomite powder by acid leaching for use in fabrication of porous ceramics, International Journal of Mineral Processing 93 (2009) 6–10.
[26] R.Q. Gao, S.L. Zheng, L.F. Zhu, Influence of tourmaline on pore structure of diatomite-based porous ceramics and malachite green decolorization, Journal of Synthetic Crystals 39 (2010) 539–543.
[27] T. Zeng, X.L. Dong, C.L. Mao, Z.Y. Zhou, H. Yang, Effects of pore shape and porosity on the properties of porous PZT 95/5 ceramics, Journal of the European Ceramic Society 27 (2007) 2025–2029.
[28] R. Guo, C.A. Wang, A.K. Yang, Effects of pore size and orientation on dielectric and piezoelectric properties of 1-3 type porous PZT ceramics, Journal of the European Ceramic Society 31 (2011) 605–609.
[29] Z.H. Lu, K.N. Sun, Preparation and characterization of silver loaded hydroxyapatite, Rare Metal Materials and Engineering 38 (2009) 56–60.
[30] B.G. Huang, G.H. Xiao, Study on assay method of silver peroxide, Gold 13 (1992) 54–57 (in Chinese).
[31] Y. Zhou, Advanced Analytical Techniques for Materials, second ed., China Machine Press, Beijing, 2006 (in Chinese).
[32] Y.H. Lv, H. Liu, Z. Wang, S.J. Liu, L.J. Hao, Y.H. Sang, D. Liu, J.Y. Wang, R.I. Boughton, Silver nanoparticle-decorated porous ceramic composite for water treatment, Journal of Membrane Science 331 (2009) 50–56.
[33] Y. Liu, X.H. Liu, X. Wang, X.D. Wu, X.J. Yang, L.D. Lu, Ag_2O nanoparticle clusters coated with porous gelatin-g-PMMA copolymer, Current Applied Physics 10 (2010) 776–782.
[34] W.N. Shen, L.J. Feng, Z.Z. Kong, Preparation of Ultrafine AgO powder and silver valence change, Rare Metal Materials and Engineering 40 (2011) 1961–1965 (in Chinese).